European Journal of Pharmaceutics and Biopharmaceutics 75 (2010) 154–161

Contents lists available at ScienceDirect

European Journal of Pharmaceutics and Biopharmaceutics

journal homepage: www.elsevier.com/locate/ejpb

Research paper

Improved membrane transport of astaxanthine by liposomal encapsulation

Chiung-Huei Peng [a], Chi-Huang Chang [a], Robert Y. Peng [a,b,*], Charng-Cherng Chyau [a,**]

[a] Research Institute of Biotechnology, Hungkuang University, Taichung Hsien, Taiwan
[b] Research Institute of Medical Sciences, Taipei Medical University, Taipei, Taiwan

ARTICLE INFO

Article history:
Received 30 July 2009
Accepted in revised form 4 March 2010
Available online 11 March 2010

Keywords:
Cell cycle arrest
Antioxidative enzymes
Hepatoma cells
Nanoencapsulation
Blood–Brain Barrier
Radiation therapy

ABSTRACT

Astaxanthine (3,3′-dihydroxy-β,β′-caroten-4,4′-dione) (AST), a red-colored carotenoid pigment, possesses extremely powerful antioxidative activity. However, its drawbacks reside in poor solubility in aqueous system, resulting in extremely low bioavailability. To ameliorate such defects, we prepared AST encapsulated within liposomes (AST-L) and tested with Hep3B and HepG2 cell lines. AST-L had size 251 ± 23 nm with AST content 89.0 ± 8.6 mg/g. AST-L apparently showed improved stability and transportability. The overall transport time was 7.55 h and 6.00 h for free AST and AST-L, respectively. AST-L more effectively activated antioxidant enzymes like superoxide dismutase, catalase and glutathione S-transferase than free AST. Hep3B consumed AST more rapidly than HepG2 cell lines. Moreover, AST-L when combined with gamma radiation (10 Gy) therapy potentially triggered subG$_1$ arrest in Hep3B and HepG2 cell lines in a dose-responsive manner ($p < 0.05$). To conclude, the poor bioavailability of AST can be improved by liposomal encapsulation, which can be a good adjuvant remedy in gamma radiotherapy.

1. Introduction

Astaxanthine (AST), chemically named 3,3′-dihydroxy-β,β′-caroten-4,4′-dione, is an exciting natural and very powerful antioxidant. It is a carotenoid pigment that is responsible for the red coloration in salmon, trout, lobsters, shrimp, flamingoes and red ocean plants. AST has a lot of uses: an antioxidant to boost immunity function, a nutraceutics to prevent heart diseases and degenerative brain damages, and a natural health remedy for sun screening [1]. AST is much more powerful than Vitamin C, E and β-carotene, a combination often used as antioxidant supplements [1]. However, its use is often limited due to its poor water solubility and extremely low bioavailability when administered orally. In reality, its antioxidative and free radical scavenging capability depend on the nature of its environmental vehicles. In octane/butyronitrile (9:1, v/v) system, it behaved as equally effective as Trolox against peroxyl radicals [2], whereas in emulsified dioleoylphosphatidyl choline liposomal suspension, it exhibited the most potent capability [2]. Commercially, AST is produced by red yeast and microalgae [2]. Literature elsewhere pointed out that AST possessed an antioxidative capability 500-fold stronger than α-tocopherol and 10-times stronger than zeaxanthine, lutein, canthaxanthine and β-carotene [3]. AST also is a promising antioxidative hepatoprotectant [4,5]. Kistler et al. demonstrated AST triggered the CYP gene expressions involving CYP3A4 and CYP2B6 and subsequently induced the cytochrome P450 (CYP) related enzymes, resulting in a very efficient *in vivo* antioxidative detoxification [6]. In food industries, AST is beneficial for edible oil preservation [7]. AST acted as a potent oxygen radical scavenger shown to be beneficial to carcinoma prognosis [7]. More recently, AST was found to effectively suppress the 6-hydroxydopamine (6-OHDA)-induced apoptosis in human neuroblastoma cell line SH-SY5Y, which in part could be attributable to its potential antioxidative capability [6,8]. To improve its bioavailability, we fabricated AST encapsulated within liposomes (AST-L). The size distribution, water dispersibility, intracellular available concentration, the expression of some relevantly related antioxidative enzymes involving superoxide dismutase (SOD), catalase (CAT) and glutathione S-transferase (GST) were examined.

Abbreviations: AST, astaxanthine; AST-L, astaxanthine encapsulated within liposomes; BNL CL2, BALB/c mouse embryonic liver cell lines; CAT, catalase; DOPC, dioleoylphosphatidyl choline; FE-SEM, Field Emission Scanning Electron Microscopy; GST, glutathione S-transferase; SOD, superoxide dismutase; Trolox, 6-hydroxy-2,5,7,8-tetramethylchroman-2-carboxylic acid; MTT, 3-(4,5-dimethylthiazol-2-yl)-2,5-diphenyl tetrazolium bromide.

* Corresponding author at: Research Institute of Biotechnology, Hungkuang University, 34, Chung-Chie Rd., Shalu County, Taichung Hsien 43302, Taiwan. Tel.: +886 2 27585767, mobile: +886 953 002 092; fax: +886 2 27585767.
** Corresponding author. Tel.: +886 4 26318652x5602, mobile: +886 932 580 897.
E-mail addresses: ypeng@seed.net.tw (R.Y. Peng), cc.chayu@msa.hinet.net (C.-C. Chyau).

0939-6411/$ - see front matter © 2010 Elsevier B.V. All rights reserved.
doi:10.1016/j.ejpb.2010.03.004

2. Materials and methods

2.1. Materials

2.1.1. Chemicals and reagents

Dulbecco's Modified Eagles Medium (DMEM), streptomycin, penicillin G, propidium iodide (PI), fetal bovine serum (FBS), MTT

(3-(4,5-dimethylthiazol-2-yl)-2,5-diphenyl tetrazolium bromide), astaxanthine, dimethyl sulfoxide (DMSO) and tetrahydrofuran (THF) were provided by Sigma Chemical Co. (St. Louis, MO, USA). Polylactide glycolic acid (PLGA) (MW ≈ 36,000) was a product of Bio Invigor Corp. (Taiwan). Polyvinyl alcohol (PVA) (MW ≈ 130,000) and egg yolk phosphotidyl choline (EYPC) were provided by Fluka AG (Buchs, Switzerland). Propidium iodide solution was prepared by dissolving propidium iodide in PBS buffer containing 0.1% v/v of Triton X-100 to a final concentration of 50 μg/mL. All other chemicals and reagents used were of analytical grade.

2.1.2. Cell lines

HepG2 and Hep3B cell lines were provided by the American Type Culture Collection (ATCC). The BALB/c mouse embryonic normal hepatic cell line (BNL CL.2 cells) was obtained from the Bioresource Collection and Research Center (BCRC, Food Industry Research and Development Institute, Hsin-Chu City, Taiwan).

2.2. Methods

2.2.1. Preparation of AST encapsulated within liposomes

Method of Pintea et al. [9] was followed with slight modification to fabricate the AST-L. Briefly, EYPC (4% w/v /DMSO) and cholesterol (1% w/v /DMSO) were dissolved in 5 mL of mixed solvent of chloroform/methanol (2:1 v/v) (S_{mix}). To the mixture, 1% of PLGA/DMSO and 1% of Tween 80/DMSO solutions and an appropriately measured amount of AST were added. Finally, a sufficient amount of S_{mix} was added to make the final concentration of AST to 1.0 mM. The solution was ultrasonicated and concentrated under reduced pressure to completely drive off the organic solvents until a membraneous product appeared on the inner wall of the concentrator. The desiccation process was continued for additional 2 h in vacuum drier. The product membrane was redissolved in 15% of ethanol/double distilled water. The solution was sonicated for 30 min with a probe Sonicator XL2020 (25 W, 20 kHz; maximum rating power, 550 W; Heat System, USA). The dispersion was filtered through a 0.2-μm membrane (produced with the LipoFast-Basic Extruder, Avestin Inc., Ontario, Canada). The filtrate was dialyzed and lyophilized to obtain AST-L.

2.2.2. Electron micrography of AST encapsulated within liposomes

Both the free liposomes and the AST-L were vacuum coated for 30 s with a gold atom layer. The morphology and size were examined at a resolution of 1.0 nm using the Field Emission Scanning Electron Microscopy (FE-SEM) (JEOL, model JSM-6500F, Japan).

2.2.3. Determination of dispersibility in aqueous medium

Fifty milligrams of free liposomes and the AST-L were accurately weighed and transferred into a 100-mL beaker to which 10 mL of PBS (pH 7.2, 30 °C) was added. The suspension was subjected to vortex for 10 min. One milliliter of which was immediately transferred to the Vial Tweenter Ultrasonic Disperser (Hielscher Ultrasonics, Esquire Biotech, Germany) and ultrasonicated for 15 min. Three ultrasonicated dispersed samples, each 10 μL, were taken and dried under the nitrogen blow. The desiccated liposomes were coated for 30 s with a gold atom layer. The number of liposome particles were counted at a resolution of 1.0 nm using the field emission Scanning Electron Microscopy (FE-SEM) (JEOL, model JSM-6500F, Japan). Similar procedure was repeated three times for each sample obtained at 0, 5 and 10 min, respectively. Data were treated statistically.

2.2.4. Measurement of disintegration time

The automatic tablet disintegrator type DISI (Charles Ischi AG, Switzerland) was used to measure the disintegration times of free liposomes and AST-L, respectively.

2.2.5. Assay of AST content in the AST encapsulated within liposomes

The AST-L (100 mg) was accurately weighed and transferred into a 100 mL beaker, to which 20 mL of PBS (pH 7.2, 30 °C) were added. The suspension was subjected to ultrasonication in the ultrasonic processor UP50H (50 W, 30 kHz (Hielscher Ultrasonics, Esquire Biotech, Germany). The ultrasonicated solution was filtered through a 0.2-μm Micropore. Ten microliters of the filtrate was subjected to the HPLC analysis as described in Section 2.2.7.

2.2.6. Stability of AST encapsulated within liposomes in different media

Free AST and AST-L were, respectively, dissolved in solvents THF and DMSO in 6-cm dishes in which these solvents had been previously placed to attain a final concentration of 20 μg/mL. The solutions were incubated at 37 °C for different time periods as indicated. The culture media were collected, to which 0.4 mL of mixed solvent (*n*-hexane:EtOH = 2:1) was added. The solution was vortexed for 1 min and then centrifuged at 1200*g* for 4 min. The *n*-hexane layer was separated and filtered through a 0.22-μm Micropore. The filtrate was subjected to HPLC analysis. The amount of AST retained in media was calculated against the calibration curve established by authentic AST.

2.2.7. HPLC analysis

For chromatographic separations the Hitachi HPLC system (Tokyo, Japan) installed with a quaternary pump (Lachrom 7100), a diode-array detector (DAD, Lachrom 7455) and an injector (M-7725i Rheodyne) attached with 20-μL loop was used. The column packed with YMC™ Carotenoid S-5C_{30} (5 μm, Waters, Milford, MA; 250 mm × 4.6 mm) was used to serve as the stationary phase. Each time an amount of 20 μL of sample solution was injected. The mobile phase consisting of dichloromethane:water:acetonitrile: methanol in ratio of 17:2:12:69, v/v was operated in an iso-gradient elution mode at a flow rate of 1 mL/min. The whole range was monitored at 480 nm. The UV span covered a spectrum from 320 to 700 nm and acquired by Hitachi D-7000 HSM software system.

2.2.8. Cell cultivation

The cell lines were incubated at 37 °C under a 5% CO_2 atmosphere in DMEM supplemented with serum. Each 500 mL of which had been previously reinforced with 10% of heat-inactivated FBS, 1% of antibiotics (penicillin 100 IU and streptomycin 100 μg) and 50 μL of 2 mM glutamine before inoculation.

2.2.9. Cellular uptake of AST encapsulated within liposomes

Hep3B and HepG2 cells were seeded onto 10-cm dishes at a density of 5×10^5 cells/mL and 1.0×10^6 cells/mL, respectively. These cultures were incubated in DMEM supplemented with serum at 37 °C for 24 h. To the cultures, 20 μg/mL of AST/THF and AST/DMSO solutions and AST-L in medium were added, respectively. The solutions were incubated at 37 °C for time durations as indicated. The cells were separately harvested and re-suspended, each in 1 mL of PBS. Two milliliters of the mixed solvent (2 mL of *n*-hexane/ethanol = 2/1, v/v) was added and ultrasonicated for 1 min. The sonificated solutions were centrifuged at 1200*g* for 4 min. The *n*-hexane layer was separated and filtered through a 0.22-μm Micropore. The filtrate was subjected to HPLC analysis. The amount of AST retained was calculated against the calibration curve of authentic AST.

2.2.10. Cytotoxicity measurement

BNL CL.2, Hep3B and HepG2 cell lines were used to examine the *in vitro* cytotoxicity of free AST and AST-L at doses as indicated. An appropriate concentration was achieved by diluting the free AST and AST-L with DMEM supplemented with serum. Cells were seeded onto a 24-well plates (Greiner Bio-One, Celistar) at a density of 2×10^4 cells/well. After 24 h the culture medium was replaced with AST solutions at different dilutions as indicated. The incubation was further continued for additional 24 h, and the cell viability was evaluated by MTT assay. To each well 50 μL of MTT solution (5 mg/mL in double distilled water) was added to yield a final concentration of 0.5 mg/mL. After incubation for 2 h, the unreacted dye was removed by aspiration. To dissolve the purple formazan product, 250 μL/well of DMSO was added. The absorbance was taken at 570 nm by a plate reader (Biomate 3, Thermo Spectronic, Madison, WI, USA).

2.2.11. Determination of intracellular antioxidant enzyme activities

BNL CL.2 cell line was cultured at a density of 5×10^6 cell/well in (DMEM supplemented with 10% of FBS in a 10-cm petri dish for 24 h. Culture media were replaced fresh and treated with different concentration of free AST and AST-L. After incubation for 24 h, the culture media were separated. Cell pellets were washed twice with cold PBS buffer and then destroyed by a probe sonicator. The cell debris with plasma was centrifuged at 13,000 rpm at 4 °C for 10 min. The protein extract (PrE) in the supernatant was separated and determined for its protein content according to Bradford [10]. The sample solution was kept at −80 °C for further use.

2.2.12. Determination of superoxide dismutase activity

The total SOD activity was determined according to Marklund and Marklund [11]. The enzyme activity expressed in U/mg protein was obtained by calculation against the calibration curve established with a standard SOD. In brief, to 40 μL of PrE 1 mL of Tris–HCl (pH 8.2) and 5 μL of 50 mM pyrogallol were added. The absorbance of the final colored solution was read in 1-min intervals at 325 nm, and the difference in optical density per minute was calculated.

2.2.13. Determination of catalase activity

Method of Cohen et al. [12] was followed with a slight modification. In brief, 40 μL of double distilled water, 50 μL of Tris–HCl-EDTA (pH 8.0) and 900 μL of 10 mM H_2O_2 were transferred into a quartz cuvette (ℓ = 10 mm). The mixture was incubated at 37 °C for 10 min. The reaction was initiated on addition of 10 μL of appropriately diluted PrE. The decrease in absorbance at 240 nm was recorded and plotted with respect to time, from which the specific activity of catalase was calculated and expressed in μmol H_2O_2/min/mg protein.

2.2.14. Determination of glutathione S-transferase activity

The activity of GST was measured according to Habig et al. [13]. An amount of 880 μL of GSH solution (1 mM GSH in 100 mM potassium PBS, pH 6.5), 95 μL of potassium PBS, 20 μL of ethanolic 1-chloro-2,4-dinitrobenzene (50 mM/EtOH) and 5 μL of PrE were transferred into a 1-mL quartz cuvette (ℓ = 10 mm). The mixture was covered with a paraffin film and slowly inverted upside down 3–4 times to facilitate the mixing. The absorbance of the colored solution was read successively at 340 nm for 2 min. A blank was performed with the similar procedure without the addition of PrE. The specific activity of GST was represented as ΔA_{340}/min/mg protein.

2.2.15. Combined effect of AST encapsulated within liposomes and gamma radiation on cell cycle arrest

A Co^{60} gamma-source (Philips SL-18 linear accelerator) supplying a gamma-emission dose-rate of 2.8 Gy/min at a total dose of 10 Gy was used for study of the damaging effect of gamma radiation on the cell cycle. Cells grown at 37 °C were treated with gamma radiation for various time intervals. The flow cytometric assay was used to track the related cell cycle perturbation. In brief, both Hep3B and HepG2 cell lines maintained in DMEM supplemented with 10% of FBS, 2 mmol/L of glutamine, 100 IU/mL of penicillin/streptomycin and 1 mmol/L of sodium pyruvate was incubated at 37 °C in a humidified incubator under 5% CO_2 atmosphere. The two cell lines were plated onto 6-cm plates at a density of 4×10^4 and 5×10^4 cells/mL, respectively, for Hep3B and HepG2. To each plate 4 mL of culture medium was added, and the cultures were incubated for 24 h to allow cell adhesion. Different concentrations of AST-L, as indicated, were added. The incubation was continued for additional 24 h before subjecting to a total dosage of 10 Gy gamma radiation. After radiation-treated, cells were further left to stand in incubator for 48 h. The irradiated cell pellets were collected and washed twice with PBS containing 1% FBS. The washed cells were successively fixed in 70% ethanol and stained with 0.5 mL of propidium iodide solution. The sample was then stored in dark at 4 °C for 30 min and filtered before flow cytometric analysis using the Coulter® Epics® XL™ Flowcytometer. Ten thousand events per sample were recorded for analysis. Data obtained were analyzed with the EXPO 32 ADC software (Beckman Coulter, Inc., CA, USA).

3. Results and discussion

3.1. Physical properties of AST encapsulated within liposomes

When microencapsulated, the size of microcapsules and the content of active constituents encapsulated will greatly affect the therapeutic effect. The common physical properties, the morphology and size are shown in Table 1 and Fig. 1. Both the free liposomes and the AST-L appeared spherical in shape having size ranging within 237 ± 45 and 251 ± 23 nm, respectively. The AST content in the AST-L reached 89.0 mg/g (Table 1). In contrast, the free AST always precipitated out in medium, agglomerating to form sizes larger than micron scale. As AST is very sensitive to oxidation, the stability of AST under different conditions was also examined. The AST-L was more stable than the free AST/DMSO and free AST/THF (Fig. 2), since the latter two were continuously exposed to the atmospheric oxygen. After standing for 25 h in the cell-free medium, the intact percentage retained at 50.0%, 33.0%, and 15%,

Table 1
Comparison of the physical properties of free AST, free liposomes and AST encapsulated within liposomes.

Properties	Free AST	Free liposomes	AST encapsulated within liposomes
Appearance/morphology	Irregular polygon agglomerate	Spheric	Spheric
Particle size distribution	>26,000 nm	237 ± 45 nm	251 ± 23 nm
Water solubility/dispersibility	Insoluble in water	Homogeneously dispersible in water	Homogeneously dispersible in water
Disintegration time, min	–	8.0 ± 2.1 min	8.0 ± 1.8 min
Content of AST	Free form, purity > 98%	None	89.0 ± 8.6 mg/g
Cell permeability	Trace amount	Freely penetrating	Freely penetrating

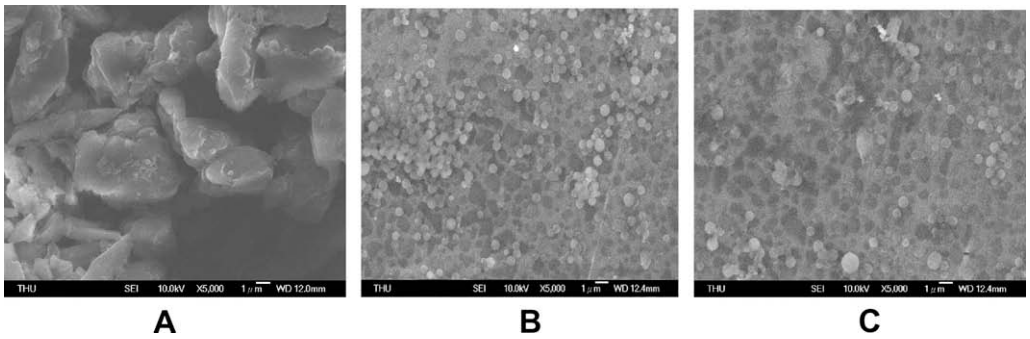

Fig. 1. FE-SEM photos of free AST, AST encapsulated within liposomes and free liposomes. Free AST (A), AST encapsulated within liposomes (AST-L) (251 ± 23 nm) (B), and free liposome only (237 ± 45 nm) (C) (magnification × 5000).

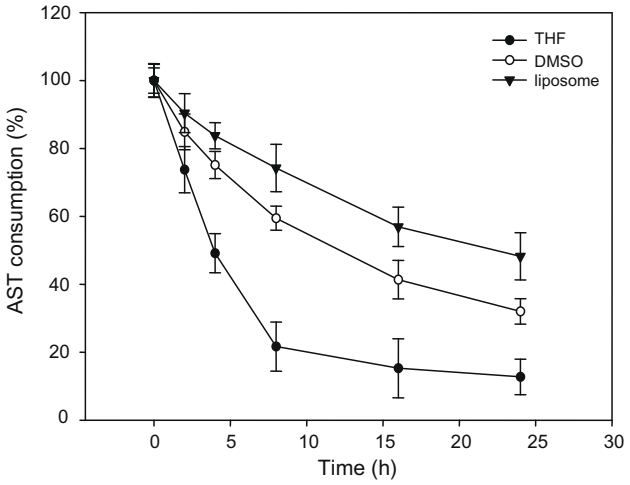

Fig. 2. Stability of free AST and AST encapsulated within liposomes. Free AST was dissolved, respectively, in THF and DMSO, and AST encapsulated within liposomes (AST-L) was dissolved in medium in a 6-cm dish to obtain a concentration of 20 μg/mL. The solutions were incubated at 37 °C for periods as indicated. To the collected medium, 0.4 mL of mixed solvent (*n*-hexane:EtOH = 2:1) was added. The solution was vortexed for 1 min and then centrifuged at 1200*g* for 4 min. The *n*-hexane layer was separated and filtered through a 0.22-μm Micropore. The filtrate was subjected to HPLC analysis.

respectively, in the AST-L, the AST/DMSO and AST/THF systems (Fig. 2), indicating prominent improvement in stability and aqueous dispersiveness resulting from encapsulation.

3.2. Bioavailability of AST encapsulated within liposomes

The bioavailability of a medicine depends on its effective uptake and consumption. Apparently, due to its nano-size and excellently

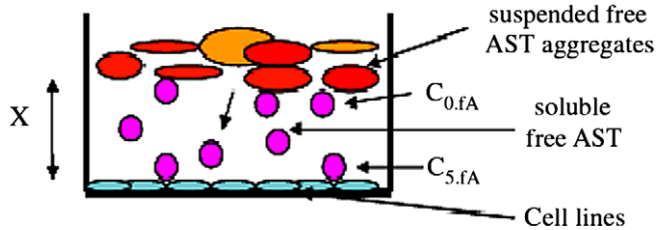

Fig. 3. The drug release kinetic model of free AST (suspended in the top layer) to the cell lines (bottom, longitudinal shape). Free AST suspended in culture medium as large aggregates having size >26,000 nm. (For interpretation of the references to color in this figure legend, the reader is referred to the web version of this article.)

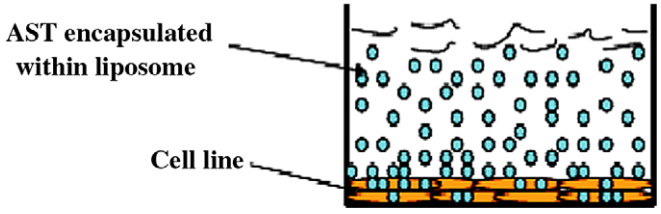

Fig. 4. The drug release kinetic model of AST encapsulated within liposomes (AST-L) (small circles) to the cell lines (bottom, longitudinal shape). Liposome particles having size 251 nm homogeneously suspended in the culture medium penetrated directly into the cell lines, and AST was then released into the cell cytoplasm. (For interpretation of the references to color in this figure legend, the reader is referred to the web version of this article.)

improved dispersiveness, the homogeneously dispersed AST-L revealed better access to the cell surfaces (Fig. 4), whereupon they readily spanned across the cell membrane and readily consumed by the cells (Table 2). As can be seen, the AST-L delivered an amount 0.29 μg AST per dish (originally seeded with 5×10^5cells) at 2 h into cell cytoplasma, much less amount was achieved by solutions of AST/THF and AST/DMSO. At 18 h, the amount of AST in Hep3B cells with AST-L reached a peak of 2.36 μg, compared to 1.17 and 0.65 μg with AST/DMSO and AST/THF solutions, respectively. Similarly, in HepG2 cell line the peak also appeared at 18 h, reaching correspondingly 1.98, 0.94 and 0.47 μg per dish (Table 2).

3.3. Kinetic parameter analysis

To explain the drug releasing kinetics, we propose two models (Figs. 3 and 4). Fig. 3 is for the free AST transport and Fig. 4 is for AST-L.

In the free AST delivery, the overall transport kinetics actually involves: (i) the dissolution time of AST from the AST aggregates, t_{dis}; where the initial concentration is $C_{0,fA}$; (ii) the diffusion of dissolved AST to the surface of cell lines adhered onto the bottom, where the concentration of AST at the cell surface is $C_{s,fA}$ and the time required is t_{dif}. Obviously, without any agitation or forced transport, $C_{s,fA}$ would be far less than $C_{0,fA}$ in magnitude and the transport would occur merely by passive transport; (iii) the transmembrane transport, which takes a time duration t_{tt}; and (iv) the consumption of AST by cell lines which will take a time t_{con} (Fig. 3). Worth noting, step iii is rather critical. As this process is not receptor-dependent, random transport will take place instead of specific delivery. In such a process, the membrane affinity and permeability may play important roles. Many cell membranes are more likely lipophilic, consequently AST may be readily bound with the membrane, hampering the membrane if not appropriately removed or consumed. Conversely, in step iv the intracellular AST

Table 2
AST uptake rate by Hep3B and HepG2 cell lines in different preparation systems.[a]

System	Incubation time, h			
	2	6	18	24
AST uptake by Hep3B cells (μg/5.0 × 10⁵ cells)				
THF	0.13 ± 0.02	0.19 ± 0.03	0.65 ± 0.27	0.06 ± 0.02
DMSO	0.17 ± 0.05	0.24 ± 0.08	1.17 ± 0.31	0.15 ± 0.04
AST-L	0.29 ± 0.09	0.55 ± 0.12	2.36 ± 0.26	0.23 ± 0.11
AST uptake by HepG2 cells (μg/1.0 × 10⁶cells)				
THF	0.12 ± 0.07	0.15 ± 0.04	0.47 ± 0.18	0.08 ± 0.01
DMSO	0.13 ± 0.05	0.18 ± 0.02	0.94 ± 0.24	0.10 ± 0.02
AST-L	0.31 ± 0.11	0.52 ± 0.14	1.98 ± 0.28	0.21 ± 0.07

[a] Hep3B and HepG2 cells were seeded onto a 10-cm dish at a cell density of 5×10^5 cells/mL and 1.0×10^6 cells/mL, respectively. Cells were incubated at 37 °C for 24 h. To the cultures, 20 μg/mL of free AST/THF, AST/DMSO solutions and AST encapsulated in liposomes/medium (AST-L) were added, respectively. The cultures were incubated at 37 °C for time durations as indicated. The cells were separately harvested, each in 1 mL of PBS. A mixed solvent (2 mL of *n*-hexane/ethanol = 2/1, v/v) was added and ultrasonicated for 1 min. The solution was centrifuged at 1200*g* for 4 min. The *n*-hexane layer was separated and filtered through 0.22-μm Micropore. The filtrate was subjected to HPLC analysis. The retention time of AST was 9.01 min (not shown). The amount of AST released into intracellular cytoplasm was calculated from the calibration curve of the authentic AST.

will be gradually consumed up by the cell lines, which will take a time duration t_{con}. Thus, the overall reaction kinetics will take an overall time.

$$\tau_{fA} = t_{dis} + t_{dif} + t_{tt} + t_{con} \quad (1)$$

In general, the time required for dissolution of water soluble solid aggregate may take only few 10 seconds to minutes and usually can be neglected. However, for highly lipophilic chemicals like AST, the dissolution time can take more than several hours. In this experiment we found it approximately to be around 0.5 h for free AST aggregates (data not shown). The dissolved AST has to traverse a distance *X* before getting access to cell surface (Fig. 3). Assume the diffusion coefficient of AST at 37 °C to be D cm^2 s^{-1}, the time required to diffuse along a distance *X* will be [14]

$$t_{dif} = X^2/2D \quad (2)$$

or

$$D = X^2/2t_{dif} \quad (3)$$

By macroscopic observation of the orange red coloration of the cell lines, the diffusion time approximately took 1.0 h (data not shown, only by judgment from microscopic observation of the coloration of cell debris). Usually, the depth of cell culture well would range within 1–2 mm depending on the volume of medium used. We measured the depth and found it to be around 1.2 mm. Substitution of this distance into Eq. (3) yielded the diffusion coefficient of free AST

Table 3
Comparison of the transport and consumption kinetic data between the free AST and the AST encapsulated within liposomes.

	Free AST	AST encapsulated within liposomes
Dissolution time h, t_{dis}	0.5	Negligible
Diffusion time h, t_{dif}	1.0	Negligible
Transmembrane time h, t_{tt}	0.05	Negligible
Consumption time h, t_{con}	6.0	6.0
Over transport time h, τ	7.55	6.0
Consumption rate of AST, μg h^{-1} $cell^{-1}$	–	–
Hep3B	–	7.1×10^{-7}
HepG2	–	3.0×10^{-7}
Diffusion rate of free AST in medium, D cm^2 s^{-1}	2×10^{-6}	–

$$D = (1.2 \times 10^{-1}\ \text{cm})^2/(2 \times 60\ \text{min} \times 60\ \text{s/min}) = 2 \times 10^{-6}\ \text{cm}^2\ \text{s}^{-1} \quad (4)$$

Next step is the transmembrane transport (step iii). In general, without receptor adaptation or endocytosis, the transmembrane uptake at least may take few minute long. We measured the intracellular concentration increase and found the t_{tt} for AST was approximately 3 min (not shown). In the final step (step iv), the intracellular consumption of AST is assumed to obey the first-order kinetics:

$$dC/dt = k_{cons}C \quad (5)$$

where k_{cons} is the consumption rate coefficient.

Depicting the data obtained during the incubation time of 18–24 h (t_{con} = 6 h) (Table 2), the consumption rates of AST by Hep3B and HepG2 cell lines based on the initial cell inoculation yielded

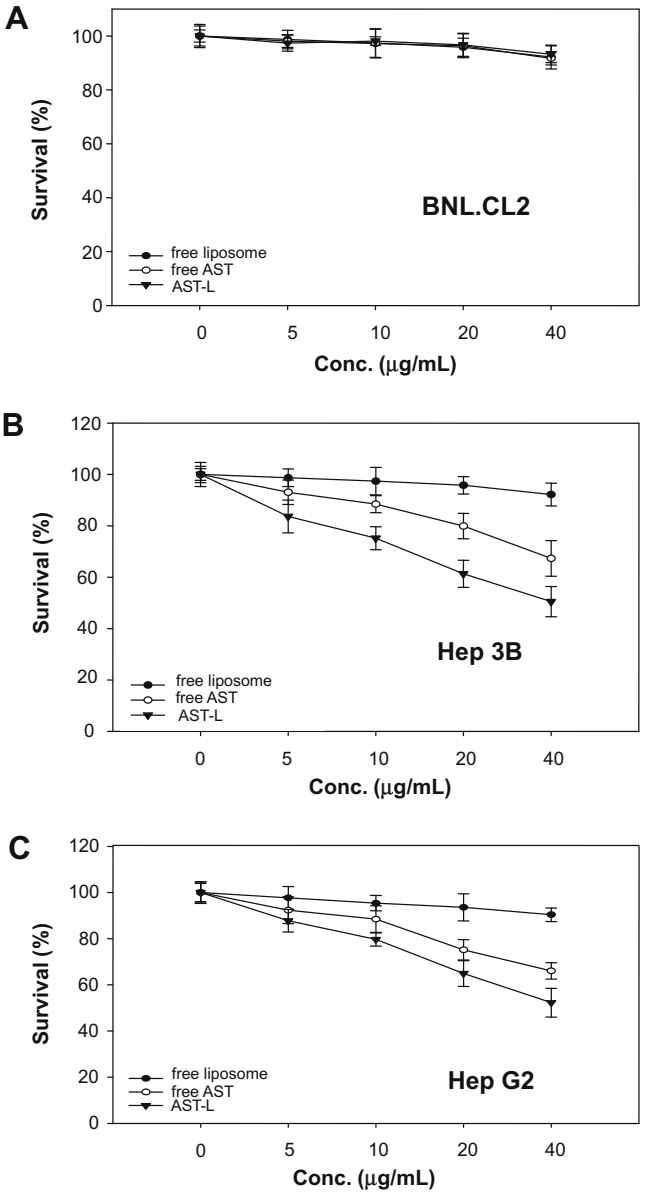

Fig. 5. MTT assay of cell viability of different cells when treated with different preparations: free AST, free liposome and AST encapsulated within liposomes (AST-L). BNL CL2 cells (A), Hep3B cells (B), and HepG2 cells (C).

7.1×10^{-7} and 3.0×10^{-7} μg h^{-1} $cell^{-1}$, respectively, indicating Hep3B was more actively consuming AST.

As a contrast, for the model of AST-L, the time intervals (t_{dis} + t_{dif}) can be neglected. As the AST-L particles are homogenously dispersed as a colloidal system, the concentration of liposome particles would be evenly distributed in the whole culture medium. Moreover, the liposome capsular materials are more lipophilic in nature, it readily adheres to cellular membrane and penetrates into cell cytoplasma due to its extremely small nano-size (251 nm); thus, the time required for transmembrane transport (t_{tt}) also can be neglected. Taking Eq. (1) as the overall model and making simplification as stated, we actually only have

$$\tau_{AL} = t_{con} \quad (6)$$

where τ_{AL} is the overall transport time for AST-L to be delivered into the cell cytoplasm. Thus, the overall reactive times will take 7.55 h and 6.0 h, respectively, by the free AST and the AST-L. The transport and consumption kinetic data of free AST and AST-L are listed in Table 3.

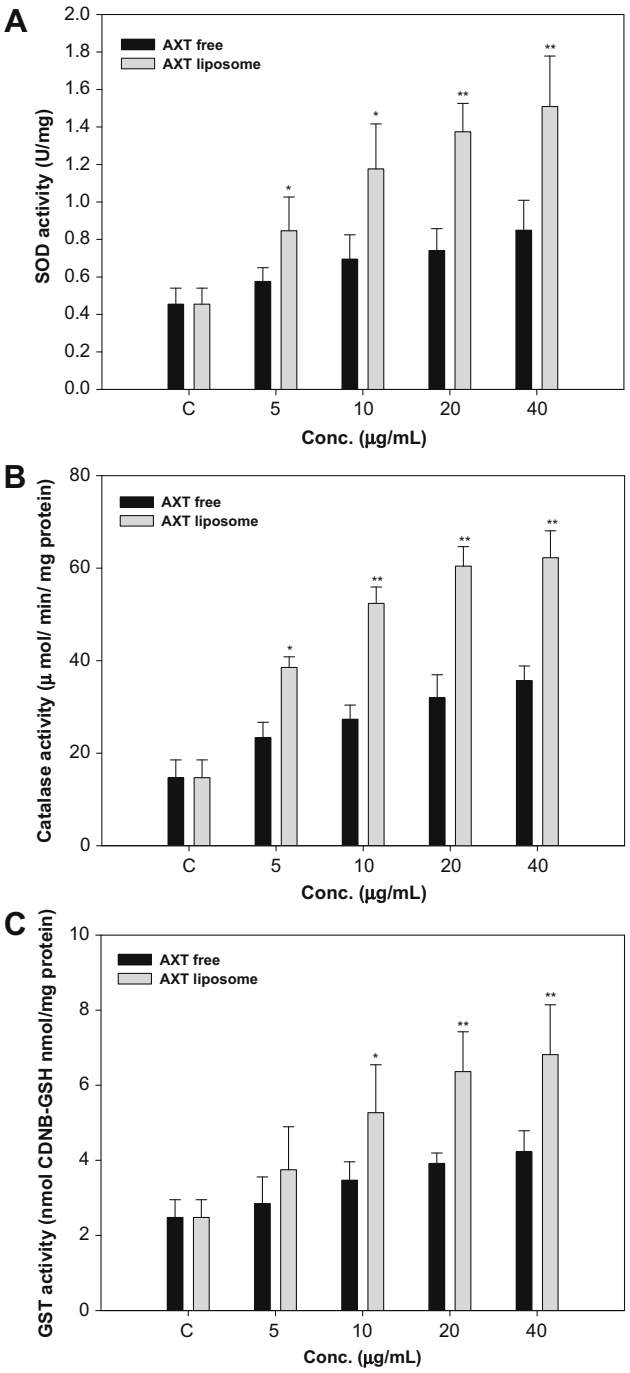

Fig. 6. Effects of AST encapsulated within liposomes on activity of SOD, CAT and GST in BNL CL.2 cell lines. Figures show activity of SOD (A), CAT (B) and GST (C) when affected in the presence and absence of AST encapsulated within liposomes (AST-L). All figures state Mean ± S.D. of triplicate experiments when tested by Student *t*-test for significance in difference ($^{*}p < 0.05$ and $^{**}p < 0.01$ vs. control group).

3.4. Cell viability affected by AST encapsulated within liposomes

AST-L was totally nontoxic to BNL CL2 cell line (Fig. 5A). In contrast, it suppressed the viability of Hep3B and HepG2 cells at 5–40 μgAST/mL in a dose-responsive manner. At 40 μg/mL, it efficiently reduced cell viability to 50% and 47%, respectively, for Hep3B and HepG2 cells. However, free AST was much less effective (Fig. 5B and C).

3.5. AST encapsulated within liposomes more effectively activated intracellular antioxidant enzymes

The activities of the target antioxidant enzymes were all apparently activated by AST (Fig. 6). At 10 μg/mL, AST-L significantly activated the three antioxidant enzymes: SOD, CAT and GST ($p < 0.05$) (Fig. 6A–C). At 20 μg/mL, the enzyme activity was increased to approximately three folds (Fig. 6A–C) ($p < 0.01$), indicating the increased dispersiveness of AST-L more effectively facilitated the mass transfer across the cell membranes.

3.6. AST encapsulated within liposomes significantly induced subG$_1$ arrest in Hep3B and HepG2 cell lines

When Hep3B and HepG2 cells were exposed to gamma radiation (RT), G_2M arrest occurred as the major perturbation in cell cycle. Alternately, when these cell lines were first exposed to AST-L and subsequently to 10 Gy of RT, the subG$_1$ phase arrest occurred in a dose-responsive manner with respect to AST-L (Table 4, Fig. 7).

As well known, phase G_0/G_1 cells contain diploids, which can last 6–12 h. Whereas cells at phases G_2 and M are characteristics of tetraploids. The former takes 3–4 h, and the latter 2 h. Whereas phase S may lasts for a period of 6–8 h. Phase subG$_1$ arrest contains in majority aneploids, during this period DNA fragmentation can

Table 4
Combined effect of AST encapsulated within liposomes and subsequent radiotherapy using gamma radiation on the cell cycle arrest and apoptosis of Hep3B and HepG2 cell lines.[a]

Treatment	SubG$_1$ (%)	G_0/G_1 (%)	S (%)	G_2/M (%)
Hep3B				
Control	1.16 ± 0.55	89.12 ± 0.19	4.93 ± 0.13	4.79 ± 0.23
RT only	6.98 ± 0.52	65.00 ± 0.59	8.12 ± 1.29	19.9 ± 1.21
AST20-RT	13.68 ± 0.76	60.65 ± 1.29	12.35 ± 2.14	13.32 ± 0.09
AST40-RT	23.49 ± 1.53	55.96 ± 0.93	8.01 ± 0.90	12.54 ± 3.35
HepG2				
Control	0.97 ± 0.37	89.63 ± 1.40	4.81 ± 0.85	4.59 ± 1.88
RT only	7.52 ± 1.14	67.01 ± 2.16	10.51 ± 1.61	14.96 ± 2.63
AST20 RT	14.24 ± 1.28	60.02 ± 0.65	10.11 ± 1.05	15.63 ± 1.68
AST40 RT	19.60 ± 1.51	57.85 ± 2.31	9.65 ± 1.82	12.9 ± 1.02

[a] The flow cytometeric data were taken by Coulter® Epics® XL™ flow cytometer (Beckman Coulter, Inc., CA, USA). Ten thousand events per sample were recorded for analysis. Data obtained were analyzed with the EXPO 32 ADC software (Beckman Coulter, CA). The cultivation condition has been stated in Fig. 5. RT: gamma radiation with 2 Gy. AST20 RT and AST40 RT: the pretreatment of cells with 20 and 40 μg AST/mL, respectively, followed by gamma radiation at a total dose of 2 Gy.

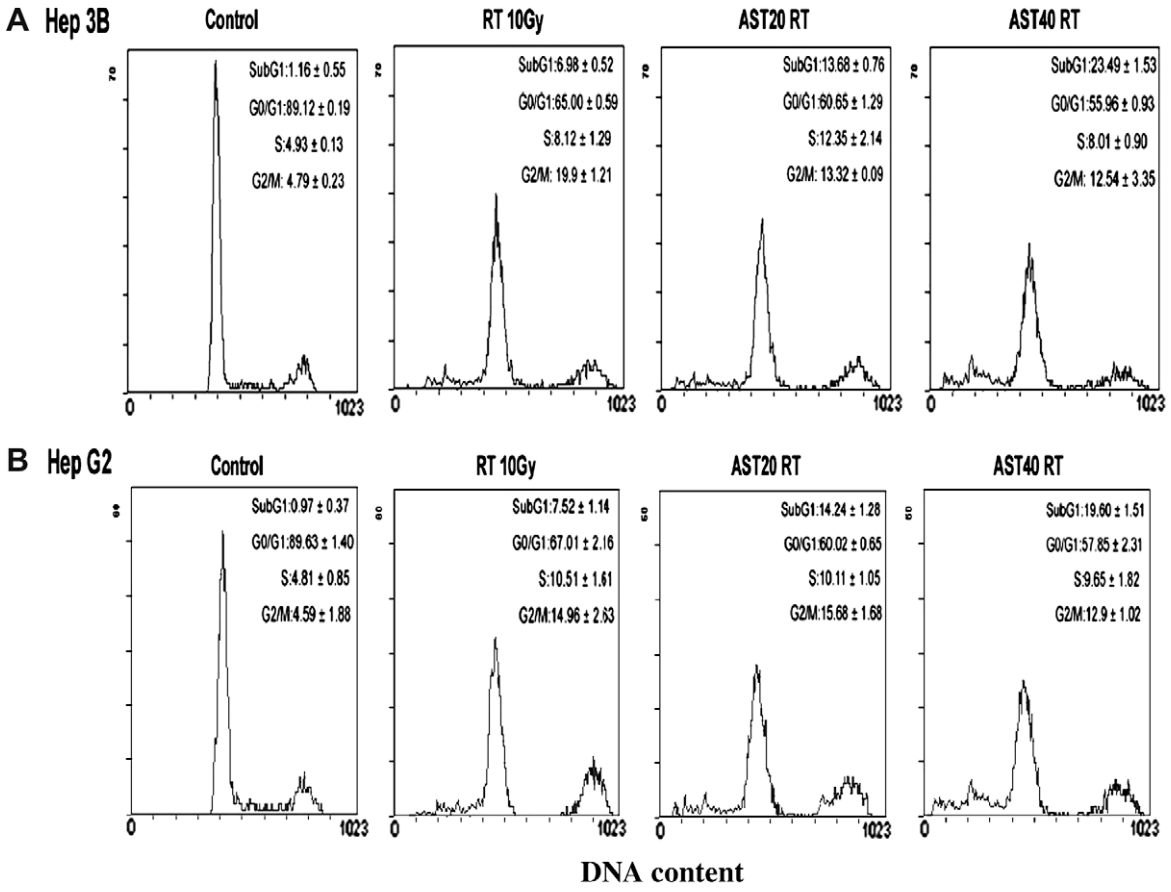

Fig. 7. Cell cycle analysis of Hep3B (A) and HepG2 (B) cells by flow cytometry in the presence and absence of AST encapsulated within liposomes (AST-L) and radiotherapy with gamma ray (RT).

be triggered by apoptosis. Results shown in Fig. 7 and Table 4 revealed that the AST-L actively induced subG$_1$ arrest and apoptosis in these hepatoma cell lines. The reasons can be ascribed to the improved membrane permeability of AST-L (Table 1). Literature elsewhere often cited that particles having size smaller than 400 nm are capable to freely penetrate the cell membrane [15,16]. In addition, the improved dispersiveness of AST-L greatly increased the availability of AST at cell membrane surface (Fig. 4), instantaneously creating effective high cytoplasmic AST concentration. The subG1 arrest induced by pretreatment with AST-L thus could be attributed to these synergistic effects (Tables 1–4, and Fig. 7). As shown, AST-L (net AST = 20 μg/mL) plus RT induced subG$_1$ arrest in Hep3B cell line. The arrested cell populations were 1.16% for the control, 13.68% by combined treatment comparing to 6.98% if treated with RT alone. The corresponding data for HepG2 cells were 0.97%, 14.24% and 7.52%, respectively (Table 4). By AST (40 μg/mL) plus RT the corresponding apoptotic percentages were further improved to 23.49% and 19.6% for Hep3B and HepG2 cell lines, respectively, in a dose-responsive manner (Table 4), implicating AST treatment effectively facilitating the apoptosis in Hep3B than HepG2 cell lines and more importantly, AST can be an excellent adjuvant therapy to improve the prognosis of RT treatment.

4. Conclusions

The poor bioavailability of astaxanthine in reality has been improved by the liposome technology. Our work implicates a general rule stating that the bioavailability of any lipophilic active principles of precious therapeutic value, like astaxanthine, in fact can be enhanced by liposomal encapsulation.

Acknowledgments

Financial support offered by the National Science Council (Taiwan) under Contract NSC-97-2313-B-241-002 is gratefully acknowledged.

References

[1] Y.M. Naguib, Antioxidant activities of astaxanthine and related carotenoids, J. Agric. Food Chem. 48 (2000) 1150–1154.
[2] R.T. Lorenz, G.R. Cysewski, Commercial potential for Haematococcus microalgae as a natural source of astaxanthine, Trends Biotechnol. 18 (4) (2000) 160–167.
[3] T. Nakano, M. Tosa M, M. Takeuchi, Improvement of biochemical features in fish health by red yeast and synthetic astaxanthine, J. Agric. Food Chem. 43 (1995) 1570–1573.
[4] E.C. Amar, V. Kiron, S. Satoh, T. Watanabe, Enhancement of innate immunity in rainbow trout (*Oncorhynchus mykiss* Walbaum) associated with dietary intake of carotenoids from natural products, Fish Shellfish Immunol. 16 (4) (2004) 527–537.
[5] A. Kistler, H. Liechti, L. Pichard, E. Wolz, G. Oesterhelt, A. Hayes, P. Maurel, Metabolism and CYP-inducer properties of astaxanthine in man and primary human hepatocytes, Arch. Toxicol. 75 (11-12) (2002) 665–675.
[6] H. Jyonouchi, S. Sun, K. Iijima, M.D. Gross, Antitumor activity of astaxanthin and its mode of action, Nutr. Cancer 36 (1) (2000) 59–65.
[7] A.R. Rao, R. Sarada, G.A. Ravishankar, Stabilization of astaxanthine in edible oils and its use as an antioxidant, J. Sci. Food Agric. 87 (6) (2007) 957–965.
[8] Y. Ikeda, S. Tsuji S, A. Satoh, M. Ishikura, T. Shirasawa, T. Shimizu, Protective effects of astaxanthine on 6-hydroxydopamine-induced apoptosis in human neuroblastoma SH-SY5Y cells, J. Neurochem. 107 (2008) 1730–1740.
[9] A. Pintea, H.A. Diehl, C. Momeu, L. Aberle, C. Socaciu, Incorporation of carotenoid esters into liposomes, Biophys. Chem. 118: (2005) 7–14.
[10] M.M. Bradford, A rapid and sensitive method for the quantitation of microgram quantities of protein utilizing the principle of protein–dye binding, Anal. Biochem. 72 (1976) 248–254.

[11] S. Marklund, G. Marklund, Involvement of the superoxide anion radical in the autoxidation of pyrogallol and a convenient assay for superoxide dismutase, Eur. J. Biochem. 47 (1974) 469–474.
[12] D. Cohen, D. Dembiec, J. Marcus, Measurement of catalase activity in tissue extracts, Ann. Biochem. 34 (1970) 30–38.
[13] W.H. Habig, M.J. Pabst, W.B. Jakoby, Glutathione S-transferase, the first enzymatic step in mercapturic acid formation, J. Biol. Chem. 249 (1974) 7130–7139.
[14] C.-H. Chang, C.-H. Peng, K.-C. Chen, H.-B. Huang, W.-T. Chiu, R.Y. Peng, Shock membrane electropotential drops and limited diffusive distance of β-amyloids in cerebral neurons are detrimental enhancement to Alzheimer's diseases, Coll. Surf. B: Biointerf. 73 (2009) 339–345.
[15] F. Yuan, M. Dellian, D. Fukumura, M. Leunig, D.A. Berk, V.P. Torchilin, R.K. Jain, Vascular permeability in a human tumor xenograft: molecular size dependence and cutoff size, J. Can. Res. 55 (1995) 3752–3756.
[16] A. Nagayasua, K. Uchiyama, H. Kiwada, The size of liposomes: a factor which affects their targeting efficiency to tumors and therapeutic activity of liposomal antitumor drugs, Adv. Drug Deliv. Rev. 40 (1999) 75–87.